2021

Exploring Mesoscale Structures using Chord Occultations of Saturn's Rings

Lamia Benyamine
University of Central Florida

EXPLORING MESOSCALE STRUCTURES USING CHORD OCCULTATIONS OF SATURN'S RINGS

by

LAMIA BENYAMINE

A thesis submitted in partial fulfillment of the requirements
for the Honors Undergraduate Thesis in Physics
in the College of Sciences
and in the Burnett Honors College
at the University of Central Florida
Orlando, Florida

Spring Term
2021

ABSTRACT

The intent of this thesis is to examine mesoscale structures found in stellar occultations of Saturn's rings. The Cassini spacecraft orbited Saturn for over 13 years and collected stellar occultations using an Ultraviolet Imaging Spectrograph (UVIS). Chord occultations were analyzed using autocorrelations at minimum ring plane radius to visualize the structure and correlation in the azimuthal direction. These particle tracking occultations cut a chord across the rings in the path of the star. By taking the autocorrelation of these chord occultations, 8 out of the 66 showed clumping within the first 3.0 km in azimuth representing signs of a structure. Six of those occultations could be moonlets or propellers as their minimum ring plane radii are in the Propeller Belt region. The Fast Fourier Transform Power Spectrum of the autocorrelation was also taken, and 6 of the 8 had high peak power outputs at certain wavelengths. It is also observed that five of the occultations may contain self-gravity wakes.

LIST OF FIGURES

LIST OF TABLES

TABLE OF CONTENTS

1. INTRODUCTION

Saturn's rings have been a scientific puzzle for centuries. Questions remain regarding their origin, evolution, and particle dynamics. Galileo Galilei first observed rings around Saturn in the seventeenth century, but every theory about their origin is challenged by their unique characteristics (Charnoz et al., 2009). In 1675, G. D. Cassini discovered a gap, now identified as the Cassini Division, which is seen as a dark band between the brighter and dimmer halves of rings A and B. About 200 years later, J. C. Maxwell proved that the rings were composed of an infinite amount of disconnected small particles that orbit about Saturn (Maxwell, 1859). These particles range in size from ~ 1mm to several meters and form a flat disk. They are primarily pure water ice with small amounts (~2%) of contaminants that give them their color (Brilliantov et al., 2015). The distribution of these particles, small moons, density waves and gaps will be used to characterize sections of the rings in this paper.

The Cassini spacecraft orbited Saturn for over 13 years, beginning in 2004, and collected stellar occultation data. Stellar occultations occur when an object passes in front of, or occults, a star. Cassini observed several bright stars as they were occulted by Saturn's ring system, providing valuable information on features of the rings (e.g. Colwell et al., 2009). This expedition's goal was to gather more information on Saturn's rings since their origin and evolution are still not entirely understood. Though the spacecraft dove into Saturn's atmosphere in 2017 so that it would not crash into one of Saturn's many moons and contaminate it with Earth microbes, research continues as many researchers dissect the extensive data set provided by the spacecraft.

This research uses Cassini Ultraviolet Imaging Spectrograph (UVIS) ring stellar occultation data. Observation methods are consistent; however, signal strength and signal-to-noise ratio vary from one occultation to the next (Esposito et al., 2004). The UVIS observed the data through two main channels, a high-speed photometer (HSP) and a hydrogen-deuterium absorption cell (HDAV). Their optical-mechanical configuration can be seen in figure 1a. The HSP was the primary channel for measuring ring structure with a sampling time of 1-2 ms (Esposito et al., 1998).

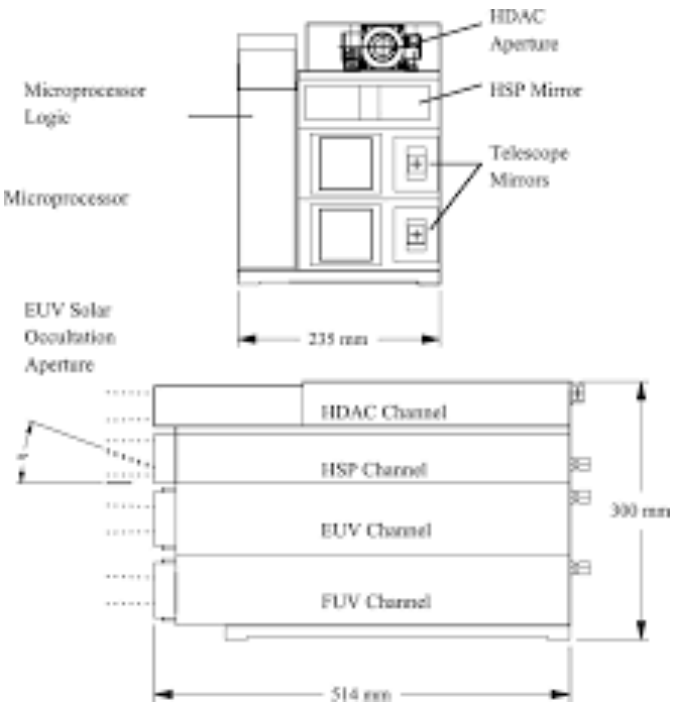

Figure 1a: Cassini UVIS mechanical characteristics with the four different channels (Esposito et al., 2004)

There are numerous distinct rings in Saturn's system, and they have been grouped into two broad classifications: dense rings (A, B, C) and tenuous rings (D, E, G). The F ring doesn't fall into these categories, but it is the narrowest of the rings and is located outside the A ring.

There is a separate ring region, the Cassini Division, that separates the A and B rings and contains more dense material. The Roche Division that separates the A and F rings comprises material similar to the D and G rings (Colwell et al., 2009). The occultation observations described in this paper are of the dense rings as well as the Cassini Division as seen in figure 1b.

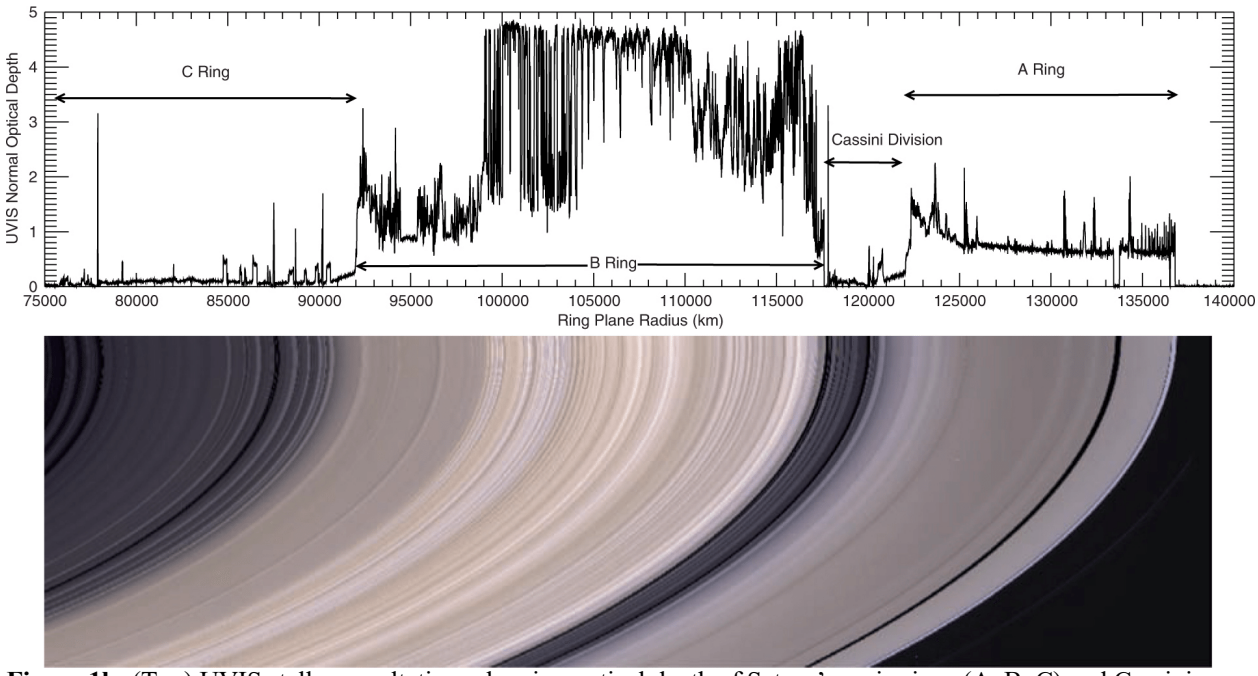

Figure 1b: (Top) UVIS stellar occultations showing optical depth of Saturn's main rings (A, B, C) and Cassini Division) at about 10 km radial resolution as a function of ring plane radius. (Bottom) A mosaic of the main rings from ISS (Colwell et al., 2009).

These regions can be described by their optical depth, (τ) which measures the opacity in the rings. An optical depth of 0 is a completely transparent ring, as the optical depth increase, more light is absorbed along its path. In these main rings, the normal optical depth (τ_n) is at least $\tau_n \geq 0.1$, which can be seen in figure 1b. The most transparent is the C ring with a varying optical depth $\tau_n \simeq 0.1$ which is similar in opacity to the Cassini Division. On the other hand, the B ring is the densest, most opaque ring and has an optical depth of $1 \leq \tau_n < 6$ (Tiscareno et al., 2019). The A ring averages $\tau_n = 1$, but has several varying peaks and dips. Azimuthal

brightness asymmetries found in the A and B ring were proven to be from the presence of density enhancements known as self-gravity wakes (Colwell et al., 2006). At the smallest scales measurable by Cassini's instruments, there are still unknown structures in the rings that are larger than individual ring particles but smaller than a few km, which we call "mesoscale" structures. Understanding all of the distinguishing features of the rings gets scientists closer to determining when and how they formed.

In this study I analyze high-resolution stellar occultations of the rings and attempt to learn more about these mesoscale structures and their underlying dynamics. This thesis will address the following tasks to answer the proposed research objectives:

1. Analysis of the structure and autocorrelation of particle tracking occultations to measure discrete azimuthal structures resolved in these occultations.
2. Investigation of periodic structures in the azimuthal direction and length scales of periodic structure from Fourier Transforms of the data.

I will describe the chord occultations used, give background on azimuthal distances, and provide details on the periodic structures that may exist in the rings. This will be followed by a detailed discussion about our methodology with the given dataset and how we came to our conclusions.

1.1 Chord Occultations

We studied the variation in structure azimuthally around the rings to focus on "chord" occultations. In these occultations, the spacecraft's line-of-sight to the star cuts a chord across the rings at various angles which is shown in figure 1.1a. At each occultation point, two angles characterize the line-of-sight orientation to the star with the rings. The ring plane opening angle (B) is the angle between the ring plane and the line-of-sight from Cassini to the star. The clock

angle (ϕ) is the angle in the ring plane from the outward radial direction to the projection into the ring plane of the line-of-sight to the star (Colwell et al., 2006). The turnaround point, or minimum ring plane radius (r_{min}), is of particular interest in our study. At this location, the intersection of the line-of-sight to the star with the rings is traveling tangent to the rings in the same direction as the ring particles' orbital motion around Saturn. This means that all measurements of the ring transparency near the turnaround point are made at the same radial distance from Saturn and provide a direct measurement of the azimuthal structure of the rings.

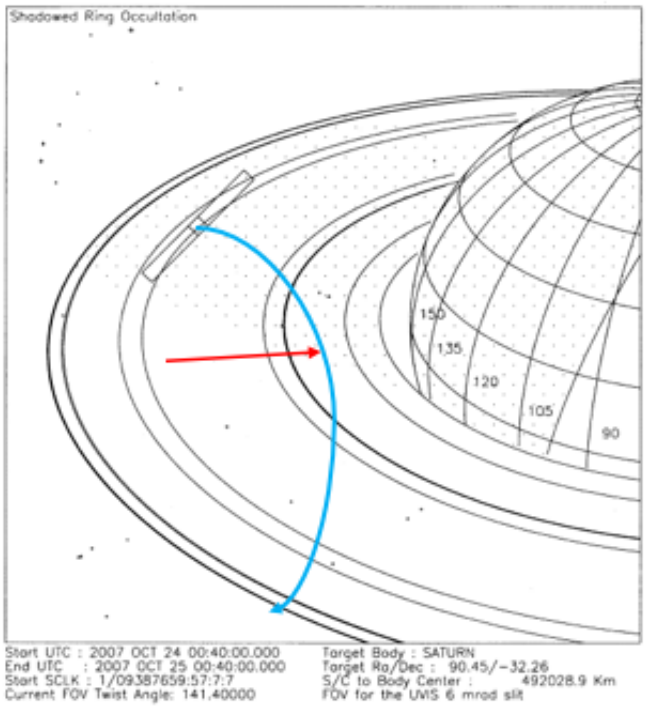

Figure 1.1a: The star ε Canis Majoris is occulted by the shadowed rings of Saturn indicated by the stippling. Also, the FUV occultation slit and HSP are shown around the star. The stippling indicated shadowed regions of Saturn and its rings (Esposito et al., 1998). The blue curve illustrates a potential path of a star behind the rings as seen from Cassini, and the red arrow shows the minimum ring plane radius sampled by this occultation. At this turnaround point, the star's distance from Saturn changes very slowly and the occultation samples change in the azimuthal or orbital direction.

1.2 Ingress and Egress

Stellar occultations are separated into ingress and egress parts. The ingress portion is when the intersection of the line-of-sight to the star with the ring plane, or intercept point hereafter, is approaching Saturn. The egress segment is where the intercept point moves away from the planet. Figure 1.2a displays the portion of a chord occultation, KapOri279, near the turnaround point, separated into ingress and egress portions. To analyze azimuthal structure in the rings, we focus our study on occultation data near the turnaround point where the ring-plane intercept point reaches its minimum radial distance from Saturn's center, and the occultation's path is tangent to the ring. Figure 1.2a also shows the data at r_{min}.

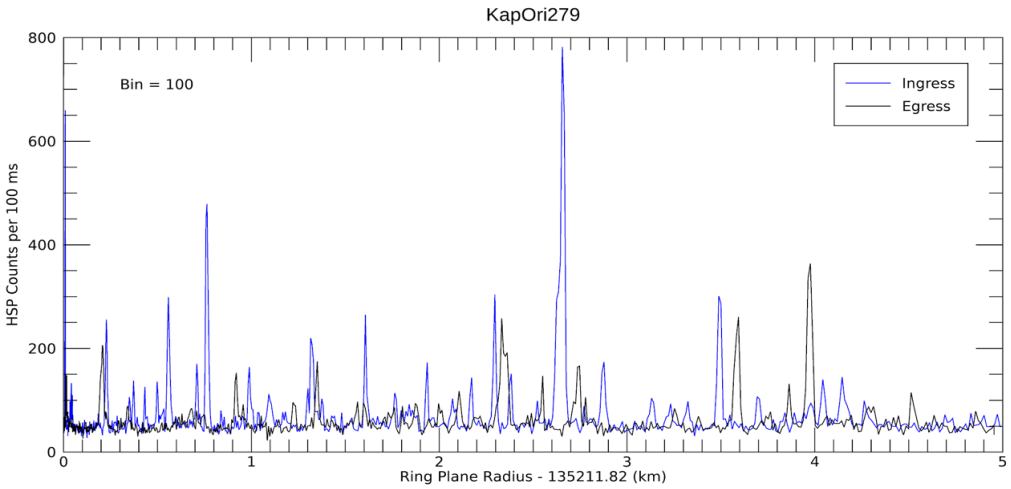

Figure 1.2a: Data from a UVIS particle tracking occultation of the star KapOri279 taken from r_{min} 123,211 km, located in the Cassini Division. Ingress (blue) and egress (red) portions of the chord occultation.

We must account for the ring particles' Keplerian orbital motion and determine the occultation point's speed relative to these particles to determine the azimuthal scale of our observations in the reference frame of the particles. This research aims to identify mesoscale

structures in Saturn's rings and determine how these structures vary with ring region and local ring properties.

1.3 Moonlets/Propellers

Small moons, moonlets, are scattered in Saturn's rings, but they cannot be directly revealed. Instead, they are detected by the larger S-shaped density structure in their surroundings, known as propellers. The moonlets that produce these structures are generally referred to as propeller moonlets or propeller objects. These propellers are small compared to the ring dimensions and are mainly located in the A ring. In figure 1.3a, a small propeller has been identified in the A ring. Moonlet wakes have been found in the azimuthal direction, downstream from the moon, thus objects only need one orbit to pass a single wake (Seiß et al., 2018). Within the A ring, there are three "Propeller Belts" located between 126,750 km and 132,000 km from Saturn's center (Tiscareno et al., 2008). There were also propeller shaped structures about 100 m in size at 125,270 km in the mid-A-ring (Tiscareno et al., 2006). Figure 1.3b displays the abundance of propellers observed, most containing a radial offset from 0.3 km - 1.4 km (Tiscareno 2008).

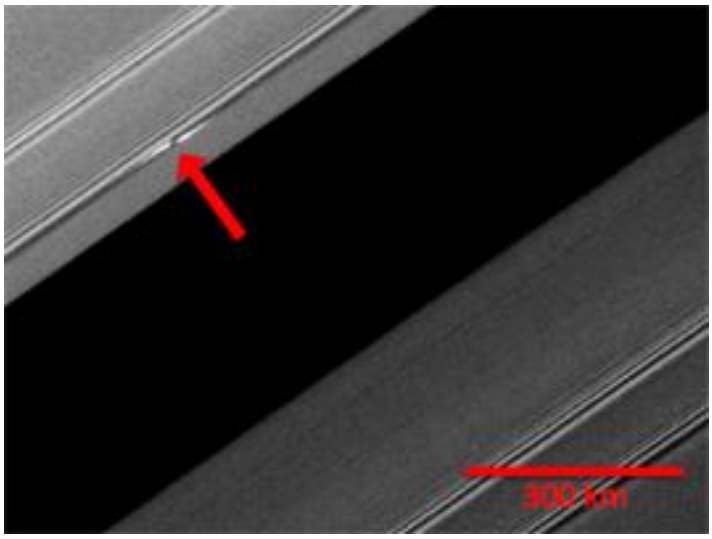

Figure 1.3a: Near the Encke Gap of the A ring, a propeller 5 km in radial dimension, 60 km in azimuthal dimension (Sremcevic et al., 2013).

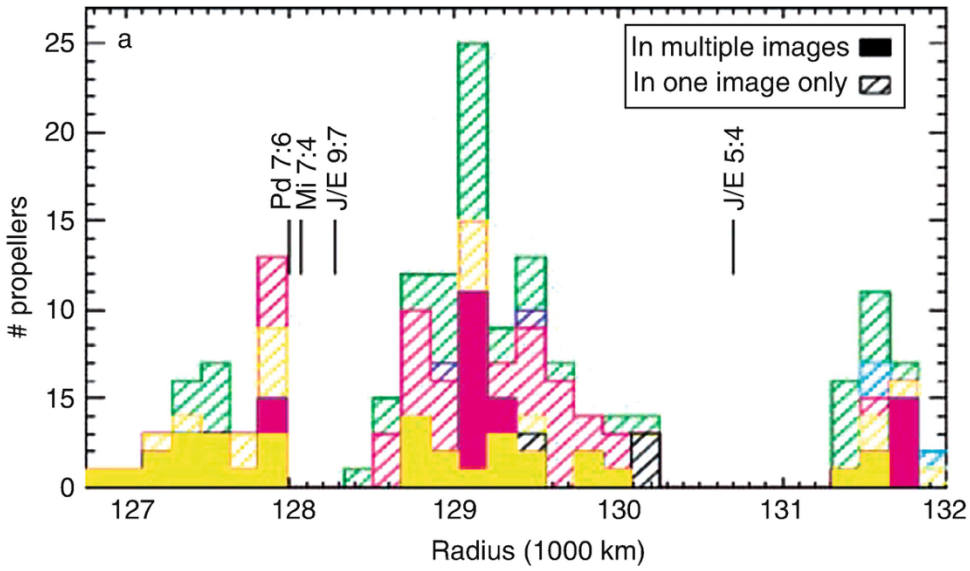

Figure 1.3b: Number of propellers against radius in the Propeller Belt regions of the A ring. Resolved propellers are noted by solid bars, and the cross-hatched bars indicate unresolved features (Tiscareno et al., 2008).

In the B ring has two categories of propellers: “big” propellers and “small” propellers. The population of “big” propellers are located in the densest part of the B ring, whereas the

"small" propellers are in the less dense portion of the inner B ring. These "small" propellers also have similar characteristics to known propellers in the A ring (Sremcevic et al., 2013).

1.4 Self Gravity Wakes

Self-gravity wakes (SGWs) are virtually opaque clumps separated by transparent gaps in the rings. The average SGW in the A ring has a cross-wake width of about 15 m and a length of 80-100 m (Colwell et al., 2006). These wakes are flatter and more closely packed in the B ring than the A ring (Colwell et al., 2007). SGWs seem to be weakly-developed or nonexistent in the Cassini Division except near 120,100 km and 120,700 km (Nicholson et al., 2010). There is a relatively featureless density wave in the A ring at 125,270 km (Tiscareno et al., 2006). The A ring has a strong correlation between locations of SGWs and optical depth (Colwell et al., 2006). On the other hand, SGWs in the B ring are less correlated with optical depth, and more so on the opening angle B. In this ring, wakes are densely packed in regions of high optical depth and more dispersed in areas of lower optical depth (Colwell et al., 2007).

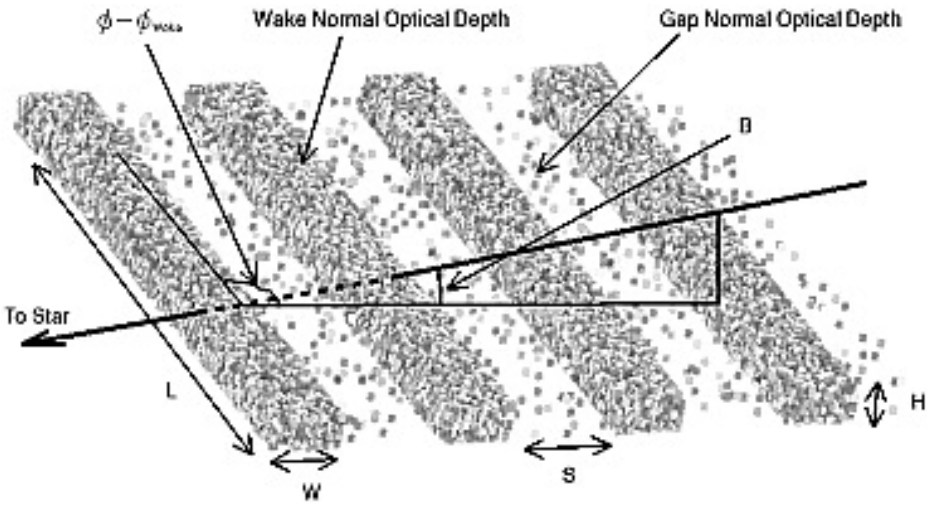

Figure 1.4a: Geometric model of self-gravity wakes displaying the parameters that affect the ring opacity. $\phi - \phi_{wake}$ is the viewing angle ϕ with respect to the wake alignment (Colwell et al., 2006).

2. METHODS

There are a few methods we used to address the research tasks. For instance, to analyze structure in the azimuthal direction, we found the chord occultations' autocorrelation. We then took the autocorrelation data and performed a Fourier transform to identify any periodicities in the data.

2.1 Dataset

The stellar occultation data is high resolution (10 to 40 m) and high signal-to-noise ratio (Esposito et al., 2004). This data consists of 276 total occultations and 66 chord occultations. The particle tracking data contains the radius, velocity, and photon counts, I, per integration period (Colwell et al., 2010). The photon count rate measures the starlight intensity; when the HSP is exposed to bright signals, I, increases rapidly for several minutes before slowing down. This measurement also includes the background noise, b, which is mainly composed of sunlight scattered by the rings (Colwell et al., 2007).

2.2 Mapping

We mapped the raw data against the ring plane radius at the turnaround point for our first effort at viewing the structures of the rings. For this procedure, it was necessary to bin the data by ~10 to 100 points to increase the signal to noise and have a uniform radial scale. This corresponds to a radial resolution of about 0.1-1.0 km for the chord occultations. We plotted the ingress and egress data in different colors to illustrate the ring structure's differences at the two different longitudes sampled by the ingress and egress portions.

2.3 Autocorrelation

Another analysis technique we used was autocorrelation, which is the degree of similarity between an occultation and a lagged version of itself over an interval. In figure 2.3a, we can see a standard cosine curve and the same curve overplotted in red shifted by a lag of 1. The autocorrelation function has a value of +1 the shifted copy of the curve and the original have a perfect positive correlation (are identical), and where the autocorrelation function has a value of 0 represents no correlation in the interval tested. In figure 2.3b, the autocorrelation was taken of the cosine curve. Using the autocorrelation in our analysis will provide evidence of periodic structure in the rings.

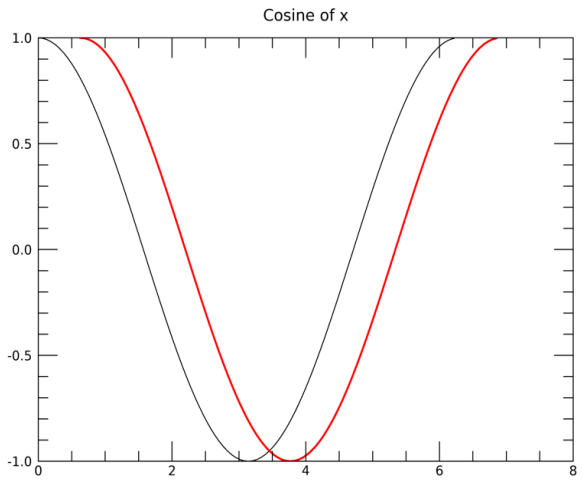

Figure 2.3a: Graph of cosine of x with a lag of 1.

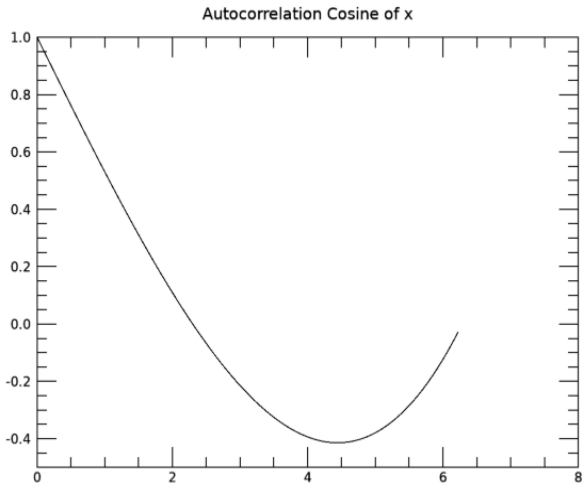

Figure 2.3b: Autocorrelation of cosine of x with a lag of 1.

We plotted the autocorrelation of the chord occultations as a function of a lag vector for our observations. This measured how much of the data set is displaced from itself in the azimuthal direction when computing the autocorrelation. Only a small subset of the autocorrelation was used to show an azimuthal distance of 0.3 km and 3.0 km. The zoomed-in correlation plot with 0.3 km azimuthal distance is useful in determining the resolution of the data

and the length for the autocorrelation to reach zero. The zoomed-out view displays any periodic structure in the rings.

2.4 Fast Fourier Transform Power Spectrum

The Fast Fourier Transform (FFT) converts signals to the frequency domain. It is also helpful in reducing background noise. The FFT Power Spectrum (FFT PS) specifically identifies periodic signals in the data. To further explore the length scales of periodic structures, the FFT PS was compiled. In figure 2.4a, the FFT PS was taken of a cosine wave with a signal creating one high frequency. In this paper we converted the frequency to display the fractional power output at each wavelength, and high-power results correspond to variations in the occultations.

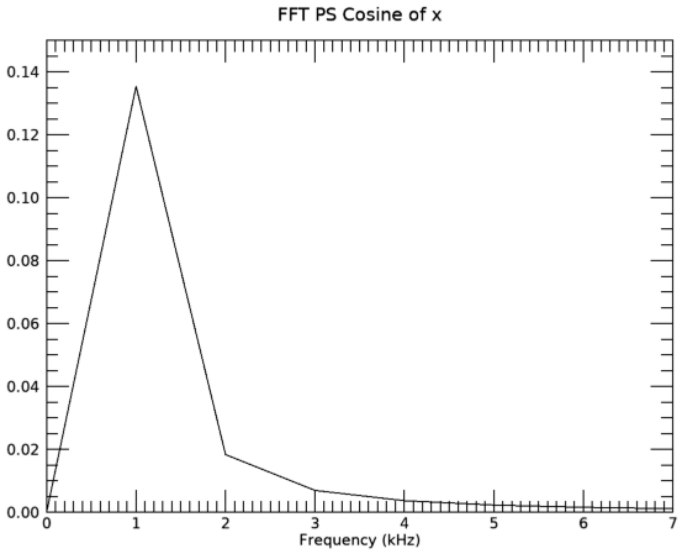

Figure 2.4a: An example FFT PS of the autocorrelation of cosine.

3. RESULTS

3.1 Azimuthal Distance

Figures 3.1a and 3.1b show the section of raw data at the turnaround point. The AlpCru100 data is binned by 100 to increase the signal-to-noise ratio. Figure 3.1b also separates the ingress and egress files to visualize how well they line up together. Typically, if the data shows a lot of noise or variation from ingress to egress, that corresponds to non-axisymmetric structure in the azimuthal direction. In figure 3.1b, several ingress peaks do not match up with their egress counterpart; thus, we observe the rings are not symmetrical at this location so there exists some structure in this occultation.

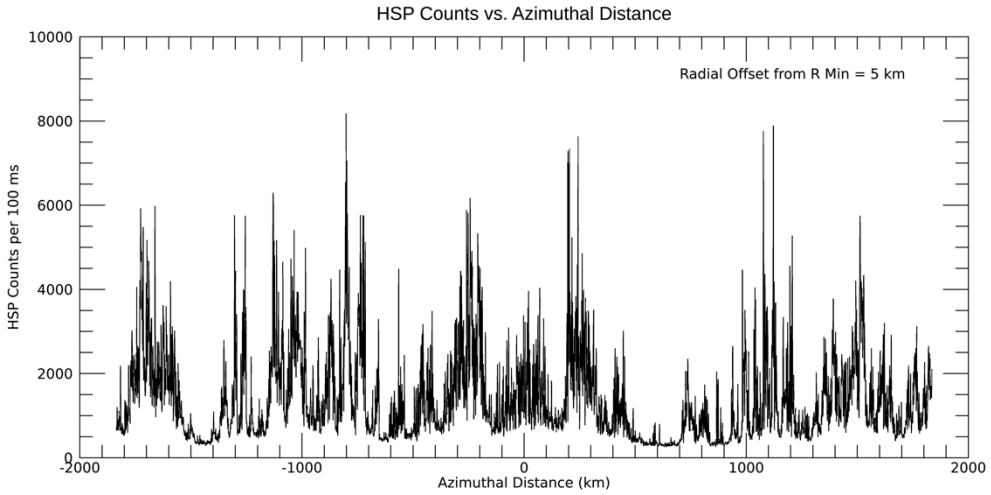

Figure 3.1a: The data of AlpCru100 within 5 km of the minimum ring plane radius in azimuthal distance.

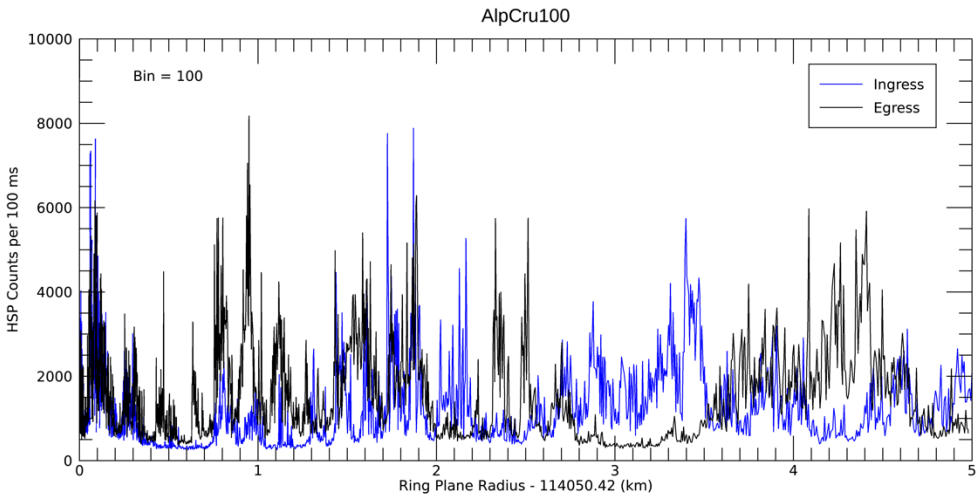

Figure 3.1b: The data of AlpCru100 at the minimum ring plane radius with separated ingress and egress data.

3.2 Autocorrelation

In figure 3.2a, the autocorrelation of AlpAra085 drops to zero after 130 meters, while KapOri280 in figure 3.2b takes a total of 300 meters to reach zero. This means AlpAra085 shows no correlation with itself once the data are offset by 130 meters. We can also view the resolution of the data in these plots. The autocorrelation of stellar occultation data from AlpAra085, shown in figure 3.2a, has just five data points with only 70 m between them. However, KapOri280 offers numerous points for the autocorrelation for the same distance. The distance between each point is 1.8 m and therefore, a higher resolution.

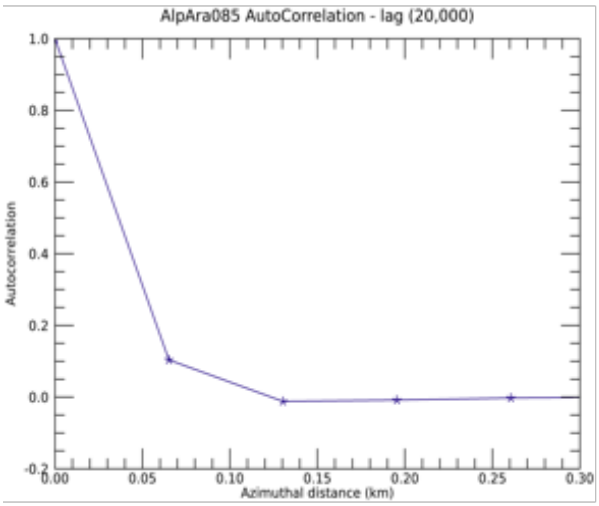

Figure 3.2a: The autocorrelation of AlpAra085 at the turnaround point with a lag of 20,000, displaying 0.3 km in the azimuthal direction.

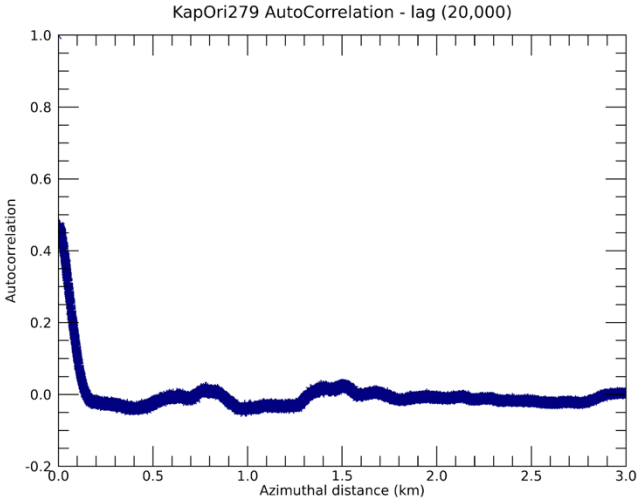

Figure 3.2b: The autocorrelation of KapOri280 at the turnaround point with the same lag and distance as 3.2a.

Figure 3.2c also has a high resolution with about 10 m in between adjacent points. This plot is interesting because after the autocorrelation reaches zero, there are various waves in the azimuthal direction. These bumps occur due to periodic structures appearing in the rings. Numerous occultations displayed similar waves after reaching zero in the autocorrelation.

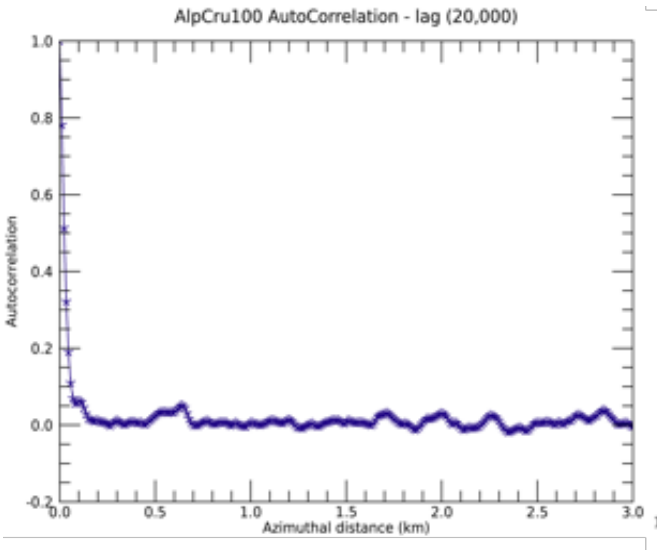

Figure 3.2c: The autocorrelation of AlphaCru100 at the turnaround point with a lag of 20,000, displaying 3.0 km in the azimuthal direction.

After analyzing all of the autocorrelation outputs, Table 3.1 lists the longest distances in azimuth before reaching zero and distinguishes the occultations that showed signs of a periodic structure. Some occultations reached zero very quickly but still showed signs of structure in that portion of the rings.

Occultation	r_{min} **(km)**	**AC drop to zero Azimuthal Distance (m)**
AlpVir008	118,979	300
KapOri280	113,448.22#	210
AlpCru100	114,050.42#	190*
DelCen064	131,696#	150*
ZetPer042	132,818.99	150
SigSgr244	130,684.112#	140*
AlpAra086	93,406.67	120
KapOri279	135,211.82#	120*
KapCMa168	130,134.12#	110*
BetPer116	131,436#	60*
BetLib187	125,891.87	60
AlpAra105	93,917.18	60
GamPeg036	102,295.56#	50*
EpsSgr247	131,510.90#	40
BetOri138	81,869.68	25
ZetCMa169	121,733.33	15*
BetOri288	80,553.76	5

Table 3.1: Lists the length in meters of azimuth that it takes for the autocorrelation to drop to zero at r_{min}. "*" indicates occultations that showed humps in the autocorrelation. "#" indicates occultations where the ingress and egress data at r_{min} are not similar.

Also, not all occultations with long radial distances corresponded to periodic structures. For instance, AlpVir008 had the most significant radial distance, shown in figure 3.2e. The

autocorrelation doesn't reach zero until about 300 m. However, the zoomed-out autocorrelation in figure 3.2f shows minimal movement after reaching zero and thus, unlikely to obtain any periodic structures. On the other hand, ZetCMa169 reaches zero very quickly, as shown in figure 3.2g, yet alternating a lot and showing possible periodic structure.

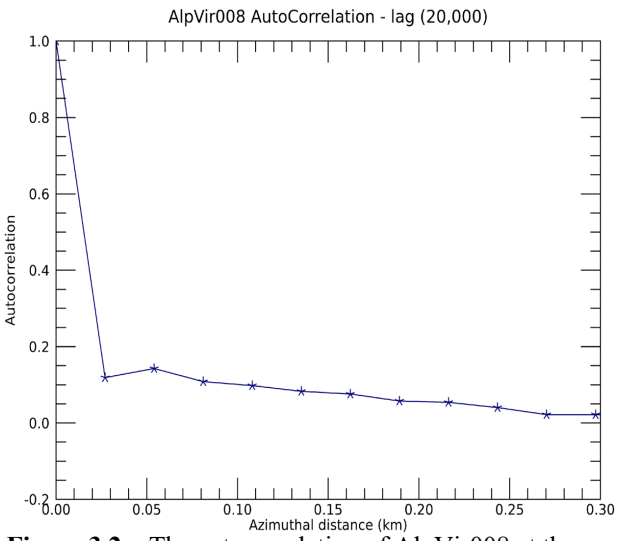

Figure 3.2e: The autocorrelation of AlpVir008 at the turnaround point with a lag of 20,000, displaying 0.3 km in the azimuthal direction.

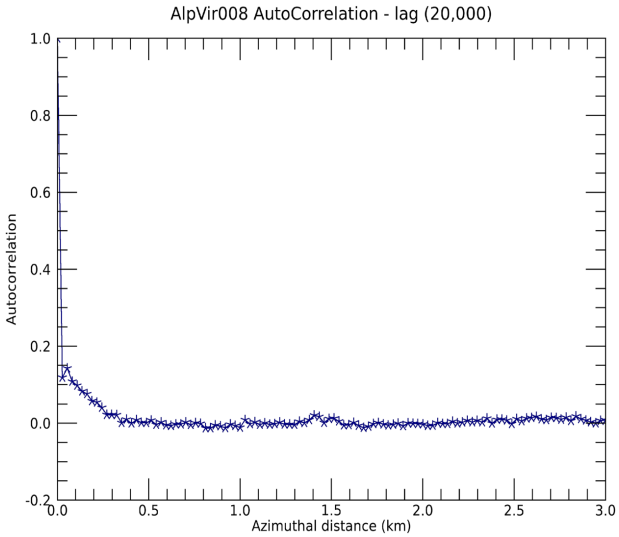

Figure 3.2f: The autocorrelation of AlpVir008 turnaround point with the same lag as 3.2e, but 3.0 km in azimuth.

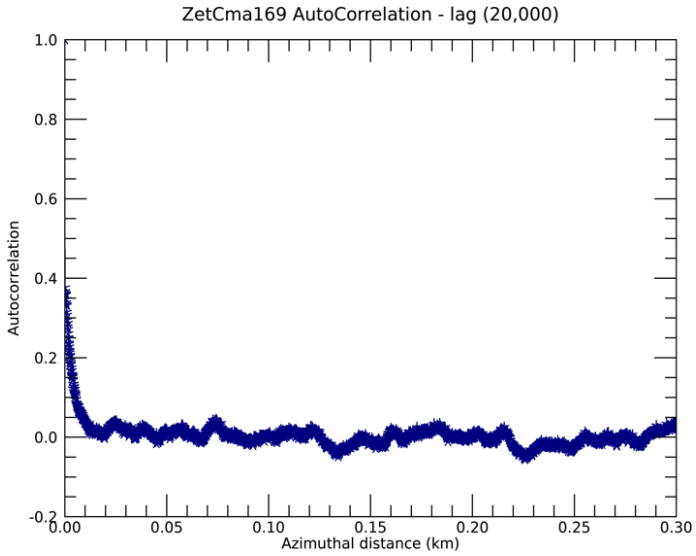

Figure 3.2g: The autocorrelation of ZetCMa169 turnaround point with a lag of 20,000 displaying 0.3 km in the azimuthal direction.

3.3 Fast Fourier Transform Power Spectrum

Standard significance calculations of the FFT show all frequencies are significant. Instead, in table 3.3 we show the two most significant wavelengths and their associated power outputs. The FFT PS of AlphaCru100 in figure 3.3a is of the entire autocorrelation data. In figure 3.3a, there is a significant spike near then of the plot, this is due to the accuracy of the FFT PS decreasing as the wavelength gets more prominent, so we used the zoomed-in version of 3.0 km, shown in figure 3.3b, for the rest of our analyses.

Occultations	**1st Peak Power Output**	**Wavelength at 1st Peak Power (km)**	**2nd Peak Power Output**	**Wavelength at 2nd Peak Power (km)**
AlpVir008	2.8×10^{-7}	1.6	2.6×10^{-7}	1.3
KapOri280	3.2×10^{-5}	2.1	2.9×10^{-5}	1.0
AlpCru100	1.6×10^{-6}	0.5	1.2×10^{-6}	0.3
DelCen064	9.5×10^{-7}	0.3	9.0×10^{-7}	1.3
ZetPer042	3.4×10^{-7}	0.5	2.4×10^{-7}	1.7
SigSgr244	4.5×10^{-6}	0.7	3.0×10^{-6}	0.6
AlpAra086	2.4×10^{-7}	0.6	1.6×10^{-7}	0.3
KapOri279	2.8×10^{-4}	0.7	1.7×10^{-4}	1.5
KapCMa168	5.5×10^{-5}	0.4	4.9×10^{-5}	0.7
BetPer116	2.1×10^{-5}	0.7	9.0×10^{-6}	0.2
BetLib187	3.6×10^{-7}	0.3	3.3×10^{-7}	0.7
AlpAra105	2.5×10^{-7}	0.4	1.1×10^{-7}	0.3
EpsSgr247	1.4×10^{-6}	0.9	1.3×10^{-6}	1.2
BetOri288	3.2×10^{-7}	0.9	1.1×10^{-7}	0.7
ZetCMa169	1.7×10^{-5}	0.1	1.5×10^{-5}	0.3
BetOri138	7.8×10^{-8}	0.5	7.5×10^{-8}	0.3

Table 3.3: Peak fractional power outputs of the FFT of the autocorrelation function.

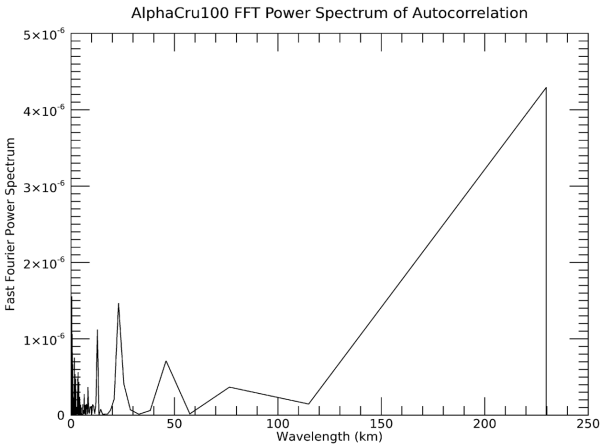

Figure 3.3a: The FFT fractional power spectral density taken of the autocorrelation of AlphaCru100 and displaying the power output at each wavelength.

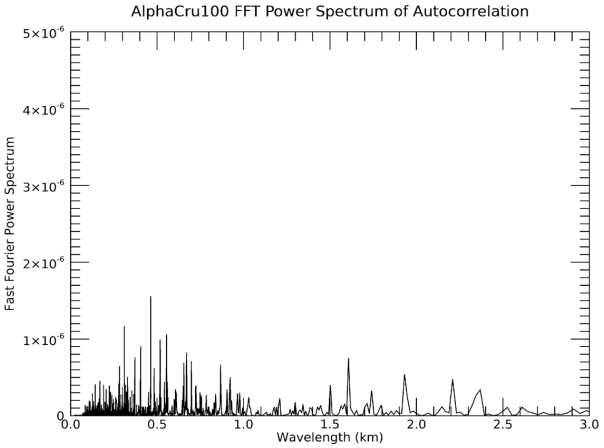

Figure 3.3b: The same FFT fractional power spectral density done in 3.3a zooming in to 3.0 km in wavelength.

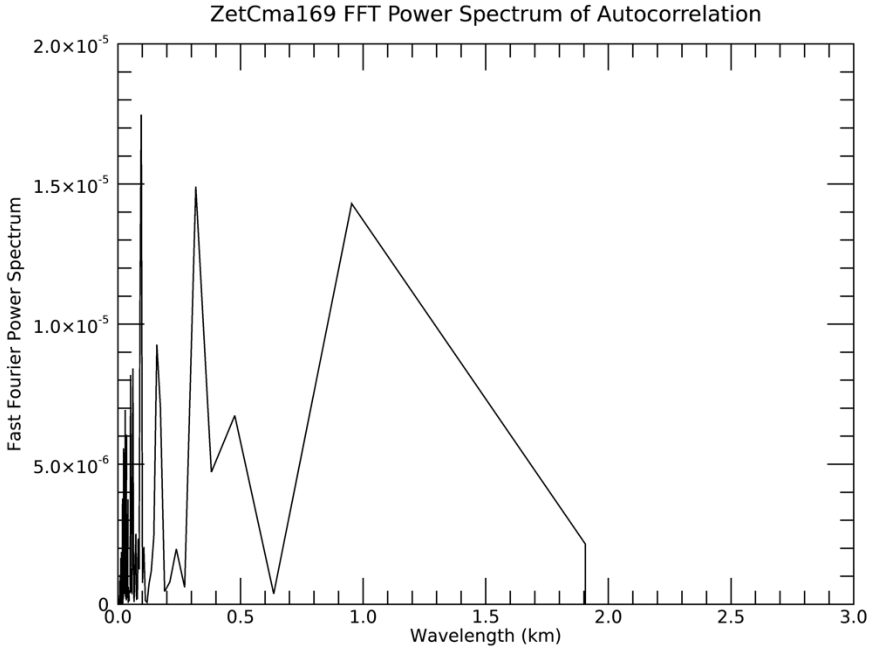

Figure 3.3c: The FFT fractional power spectral density taken of the autocorrelation of ZetCMa169 and displaying the power output at each wavelength zooming in to 3.0 km in wavelength.

Figure 3.3b shows low and stable power outputs across 3.0 km of wavelength. This provides evidence that there are most likely not any periodic structures in this distance, even with the very wavy autocorrelation shown in figure 3.2c. However, figure 3.3c outputs a high range of

power at various wavelengths along the same stretch. The highest peak reaches about 1.7×10^{-5} fractional power at 0.1 km and a similar power output at 0.3 km. This high power could be periodic structures, but more analysis is needed to come to a conclusion. We analyzed all of the provided chord occultations and used the results to determine which occultations may contain mesoscale structures.

4. DISCUSSION

We found variations in Saturn's main rings that suggests that various structures exist in the observed chord occultations. The ring plane radius plots displayed 8 occultations that showed variations between the ingress and egress data. After analyzing the autocorrelation, within the first 3.0 km in azimuthal distance, eight occultations showed clumping, thus signs of a non-asymmetric structure. These structures range in size from about 15 m to 190 m in azimuth. Six of the occultations could be moonlets or propellers as their minimum ring plane radii are in the Propeller Belt region of the A ring. These possible propellers are in BetLib187, KapCMa168, SigSgr244, BetPer116, EpsSgr247, and DelCen064 which can be seen in figure 4a with the summary of possible structure in the observed occultation. The B ring does not have as large of an identified region of propellers but based on the change in optical depth in the B ring, occultations KapOri280 has an r_{min} in an area of identified propellers. There is about 400 m between an ingress and egress peak in the radius plot, this size structure could be a large propeller. AlpAra105 is in a location that is similar in optical depth to the A ring that has identified propellers, therefore, it could also be a propeller.

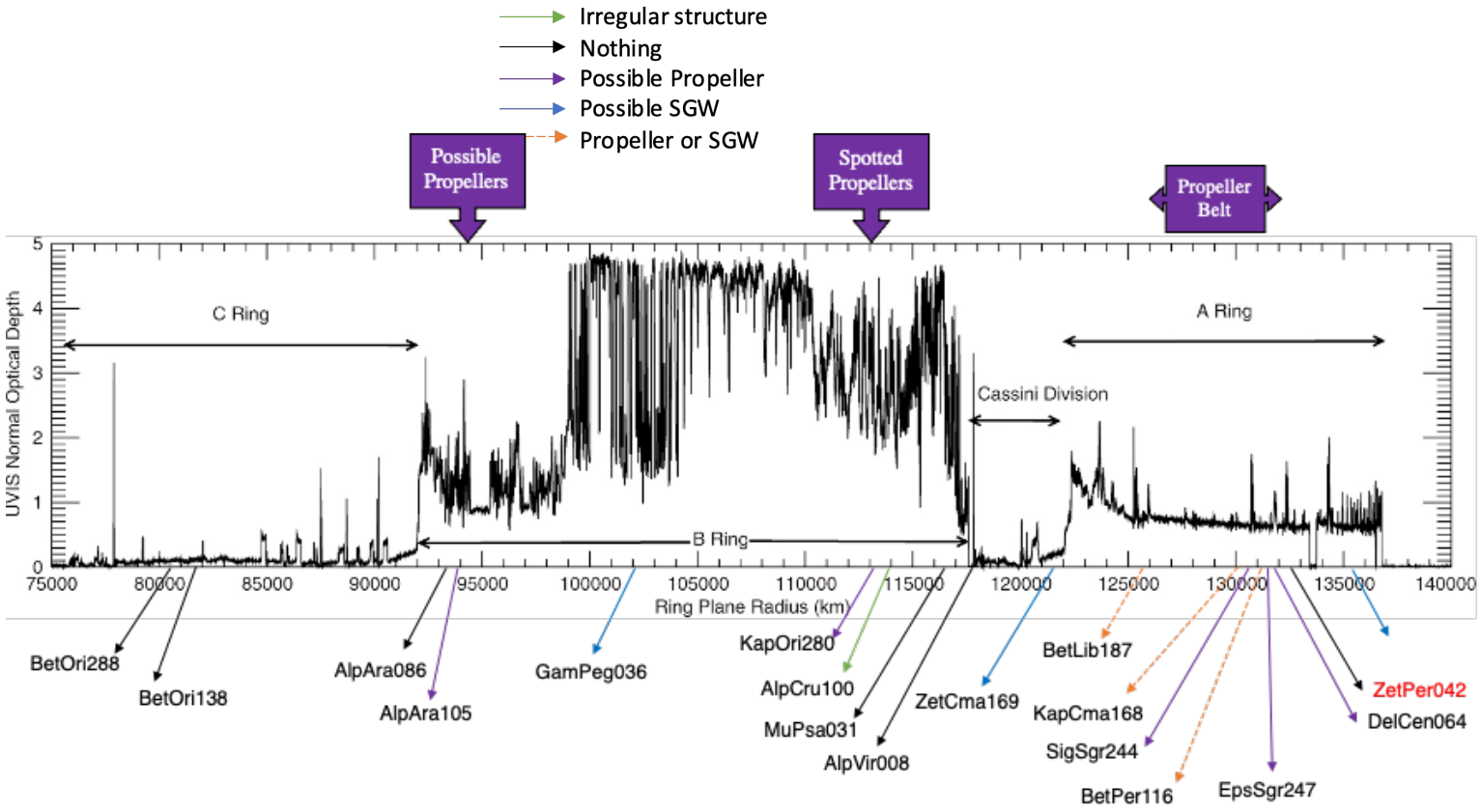

Figure 4a: Displaying the main rings along ring plan radius with labeled possible structures in the observed. occultations

About six occultations could be characterized as having SGWs based on the characteristics shown in their ingress and egress data. There seems to be some order to the offset peaks in the two data sets, for instance, KapOri279 has two sets of ingress and egress peaks with about 10 m distance between wakes. This demonstrates the common gap-wake characteristic of SGWs. GamPeg036 has several matching peaks of various sizes about 5 m in distance. Above, BetLib187 is identified as a possible propeller, but based on previous literature, the r_{min} is also located in a density wave. There is about 10 m of distance between peaks and wakes and so it may be a SGW. KapCMa168 is in a Propeller Belt, but it also shows signs of being a SGW. The distance between peaks is about 5 m. These chord occultations and more could be possible SGW.

Some other observations were that AlpCru100 is not in any known structural locations, but it has one of the larger gaps in autocorrelation to reach zero, about 190 m in azimuth. It also has a peak power output around 400 m in wavelength so there is some periodic structure in this occultation. ZetCMa169 has an r_{min} in the Cassini Division only has structure about 15 m in azimuth and has very low power outputs from the FFT, but the autocorrelation showed a lot of humps after it reached zero. However, it is located near a region of SGWs, so it is possible it has more characteristics that need to be explored. Further analyses of the chord occultations, can determine other possible structures in the main rings.

5. REFERENCES

Brilliantov, N., Krapivsky, P. L., Bodrova, A., Spahn, F., Hayakawa, H., Stadnichuk, V., & Schmidt, J. (2015). Size distribution of particles in Saturn's rings from aggregation and fragmentation. Proceedings of the National Academy of Sciences, 112(31), 9536–9541. https://doi.org/10.1073/pnas.1503957112

Charnoz, S., Esposito, L., Estrada, P. R., Hedman, M. M., & Dones, L. (2009). Origin and Evolution of Saturn's Ring System. In: Dougherty M.K., Esposito L.W., Krimigis S.M. (eds) Saturn from Cassini-Huygens. Springer, Dordrecht, 537–575. https://doi.org/10.1007/978-1-4020-9217-6_17

Colwell, J. E., Esposito, L. W., & Sremčević, M. (2006). Self-gravity wakes in Saturn's A ring measured by stellar occultations from Cassini. Geophysical Research Letters, 33(7). https://doi.org/10.1029/2005gl025163

Colwell, J. E., Esposito, L. W., Jerousek, R. G., Sremčević, M., Pettis, D., & Bradley, E. T. (2010). Cassini UVIS Stellar Occultation Observations of Saturn's Rings. The Astronomical Journal, 140(6), 1569–1578. https://doi.org/10.1088/0004-6256/140/6/1569

Colwell, J. E., Nicholson, P. D., Tiscareno, M. S., Murray, C. D., French, R. G., & Marouf, E. A. (2009). The Structure of Saturn's Rings. Saturn from Cassini-Huygens, 375–412. https://doi.org/10.1007/978-1-4020-9217-6_13

Colwell, J., Esposito, L., Sremčević, M., Stewart, G., & Mcclintock, W. (2007). Self-gravity wakes and radial structure of Saturn's B ring. Icarus, 190(1), 127–144. https://doi.org/10.1016/j.icarus.2007.03.018

Esposito, L.W., Barth, C.A., Colwell, J.E. et al. (2004). The Cassini Ultraviolet Imaging Spectrograph Investigation. Space Sci Rev 115, 299–361. https://doi.org/10.1007/s11214-004-1455-8

Esposito, L. W., Colwell, J. E., & Mcclintock, W. E. (1998). Cassini UVIS Observations of Saturn's Rings. Planetary and Space Science, 46(9-10), 1221–1235. https://doi.org/10.1016/s0032-0633(98)00076-2

Maxwell, J. C. 1859. On the stability of Saturn's rings (London). Reprinted in The Scientific Papers of James Clerke Maxwell,2Vols. 1890. University of Cambridge Press, Cambridge, pp. 288–374.

Nicholson, P. D., & Hedman, M. M. (2010). Self-gravity wake parameters in Saturn's A and B rings. Icarus, 206(2), 410-423. https://doi.org/10.1016/j.icarus.2009.07.028

Seiß, M., Albers, N., Sremčević, M., Schmidt, J., Salo, H., Seiler, M., … Spahn, F. (2018). Hydrodynamic Simulations of Moonlet-induced Propellers in Saturn's Rings: Application to Blériot. The Astronomical Journal, 157(1), 6. https://doi.org/10.3847/1538-3881/aaed44

Sremcevic, M., Stewart, G. R., Albers, N., & Esposito, L. W. (2013), Propellers in Saturn's rings, AGU, Fall Meet., Abstract P21E-07.

Tiscareno, M. S., Burns, J. A., Hedman, M. M., & C. Porco, C. (2008). THE POPULATION OF PROPELLERS IN SATURN'S A RING. *The Astronomical Journal*, *135*(3), 1083–1091. https://doi.org/10.1088/0004-6256/135/3/1083

Tiscareno, M. S., Burns, J. A., Hedman, M. M., Porco, C. C., Weiss, J. W., Dones, L., … Murray, C. D. (2006). 100-metre-diameter moonlets in Saturn's A ring from observations of 'propeller' structures. Nature, 440(7084), 648–650. https://doi.org/10.1038/nature04581

Tiscareno, M. S., Nicholson, P. D., Cuzzi, J. N., Spilker, L. J., Murray, C. D., Hedman, M. M., … Sotin, C. (2019). Close-range remote sensing of Saturn's rings during Cassini's ring-grazing orbits and Grand Finale. *Science*, *364*(6445). https://doi.org/10.1126/science.aau1017